Materials Science and Engineering B 163 (2009) 114–119

Contents lists available at ScienceDirect

Materials Science and Engineering B

journal homepage: www.elsevier.com/locate/mseb

Geometry effects on magnetoelectric performance of layered Ni/PZT composites

D.A. Pan[a,*], J.J. Tian[a], S.G. Zhang[a], J.S. Sun[b], A.A. Volinsky[c], L.J. Qiao[a]

[a] School of Materials Science and Engineering, University of Science and Technology Beijing, Beijing 100083, PR China
[b] Faculty of Materials and Metallurgical Engineering, Kunming University of Science and Technology, Kunming, Yunnan, 650093 PR China
[c] Department of Mechanical Engineering, University of South Florida, Tampa, FL 33620, USA

ARTICLE INFO

Article history:
Received 25 November 2008
Received in revised form 6 May 2009
Accepted 24 May 2009

Keywords:
Functional composites
Layered structures
Vibration
Magnetoelectric properties

ABSTRACT

Layered magnetoelectric (ME) composite structures of varying geometry consisting of PZT and Ni layers were prepared by electrodeposition. Trilayered plate, bilayered and trilayered cylindrical structures' ME performance was compared. The ME voltage coefficient increased with Ni layer thickness. Cylindrical composites show better ME performance than the plate structures with the same magnetostrictive-piezoelectric phase thickness ratio under high applied magnetic fields at resonant frequencies. Bilayered cylindrical Ni/PZT structure has the best performance in axial mode under high magnetic field, exhibiting linear ME voltage coefficient dependence on the applied magnetic field, which makes it a promising candidate for magnetic field sensor applications. Cutting the ring along the axial direction drastically decreased its performance.

1. Introduction

Layered multiferroic materials are candidates for the next-generation multifunctional devices [1–6]. In these structures, the interaction between ferroelectric and ferromagnetic layers produces new coupled magnetoelectric (ME) effect [7,8]. The ME response appears as an electric polarization upon applying magnetic fields and/or a magnetization upon applying electric fields, and has been observed in some single-phase materials [9,10], including $BiFeO_3$ and $BaMnF_4$ [11,12]. The ME effect comes from the local exchange between the internal orderly magnetic structure and ferroelectric sub-lattice [13]. Unfortunately, single-phase materials exhibit weak ME effect, which explains their limited application. Magnetoelectric layered composite structures provide an alternative, exhibiting higher ME effect due to mechanical coupling between piezoelectric and ferromagnetic layers [14]. When magnetic filed is applied to the ferromagnetic layer, it deforms, transporting mechanical strain onto the piezoelectric layer, thus generating an electric potential. The magnetoelectric coefficient is the voltage generated in the piezoelectric due to the applied magnetic field per piezoelectric thickness, and has the units of V/(cm Oe). Ferroelectric and ferromagnetic layered materials have Curie and Neil temperatures above room temperature, and exhibit larger piezoelectric and piezomagnetic effects compared with traditional single-phase ME materials.

There are two major types of synthesized ME composites: particulate and layered composites. Particulate composites include sintered and organic solidified composites [15–20]. The ME effect is weak in these sintered structures because of the diffusion between phases and the seepage phenomenon. The same problem exists with organic solidified composites made by hot pressing of piezoelectric and piezomagnetic granular materials.

Layering has become a popular method for synthesizing ME composites. This is especially true for joining together piezoelectric and piezomagnetic phases by bonding or hot pressing [21–28]. The ME effect in layered composites is much higher compared with the particulate composites made from the same materials [29]. However, interfacial effects in laminate composites are inevitable, and constrain the improvement and applications of ME laminate composites due to ageing and fatigue.

Liu and co-workers made layered composites with improved ME effect by bonding layers of varying geometry [30]. However, based on the limitation of the gluing method, only simple planar shapes could be produced, including laminated squares and disks [31,32]. Laletin et al. reported the giant ME effect in layered transition metal/PZT samples synthesized by bonding thin disks of PZT and Fe, Co or Ni with an adhesive [33]. As for more complex shapes, such as cylinders, new techniques had to be developed. It is possible to improve the ME layered composite performance by depositing each layer directly, without the use of a bonding agent, which provides much better mechanical coupling and can produce more complex shapes that will help improve the ME effect.

Electrodeposition is widely used for making composite functional materials with good interfacial adhesion. Electrodeposition process has the ability to coat complex shapes, while controlling coating thickness and composition [34–36]. Magnetic materials, including Fe, Co, Ni and their alloys can be deposited by electrodeposition from the corresponding salt solutions. Moreover, the

* Corresponding author. Tel.: +86 10 82376835; fax: +86 10 62333375.
E-mail address: pandean@mater.ustb.edu.cn (D.A. Pan).

0921-5107/$ – see front matter © 2009 Elsevier B.V. All rights reserved.
doi:10.1016/j.mseb.2009.05.017

bonding glue layer can be avoided with this method. We utilized electrodeposition to make layered ME composites with complex shapes and improved ME properties, which are discussed later.

2. Experimental procedures

Three different structure types were made, and include planar trilayered Ni/PZT/Ni, cylindrical trilayered Ni/PZT/Ni, and cylindrical bilayered Ni/PZT composites, presented schematically in Fig. 1. Commercial PZT-5H ceramic ($Pb(Zr_{0.52}Ti_{0.48})O_3$ supplied by the Institute of Acoustics, Chinese Academy of Sciences) was utilized as the piezoelectric layer and electrodeposited pure nickel (Ni) was utilized as the magnetic layer, which had good piezoelectric properties. The main performance parameters of PZT-5H are shown in Table 1.

Sample preparation consisted of the following steps: first, the PZT was mechanically cut into desired shape, then polarized (vector P shows the polarization direction in Fig. 1), and then bathed in a plating solution to electrodeposit Ni. The thickness of Ni was controlled by the deposition time. For a plate layered ME composite, shown schematically in Fig. 1(a), the dimensions of PZT center layer are $W \times L \times t_{PZT} = 10\,mm \times 20\,mm \times 0.25\,mm$, where t_{PZT} is the thickness of PZT. Varying thickness Ni layers were electro-plated on both sides of the PZT samples. The deposition times were 1, 2 and 4 h, which resulted in 0.1, 0.2 and 0.4 mm thick Ni layers, respectively.

For the cylindrical trilayered ME composite, shown schematically in Fig. 1(b), the dimensions of PZT are $R_1 \times R_2 \times h\,mm^3$, where $R_1 = 9$ mm is the inner radius, $R_2 = 10$ mm is the outer radius, $h = 8$ mm is the PZT cylinders height and $t_{PZT} = (R_2 - R_1)$. Ni was deposited on both inner and outer PZT cylinder surfaces for 10 h, which resulted in total 1 mm Ni layer thickness (0.5 mm on each side of the cylinder). For the cylindrical bilayered structure, shown schematically in Fig. 1(c), the PZT cylinder height is 3 mm ($h = 3$ mm), and the other two dimensions are the same as for the trilayered cylindrical structure ($R_1 = 9$ mm $R_2 = 10$ mm). The corresponding PZT radii are R_1 and R_2 shown in Fig. 1(c). Besides having smaller height compared with the trilayered cylindrical structure, Ni was only deposited on the outer PZT cylinder surface for 20 h, resulting in 1 mm Ni layer thickness. For both cylindrical samples, PZT was polarized in the radial directions (P in Fig. 1(b) and (c)).

Ni electrodeposition process is described in detail elsewhere [37]. Nickel aminosulfonate plating solution (concentration of 600 g/L) was used due to its stability, rapid plating speed and small film residual stresses. Nickel chloride (20 g/L) was added to the plating bath to help the anode dissolution. Boric acid (20 g/L) acted as a buffer to stabilize the plating solution pH. The pH value was adjusted to 4 by using sulfamic acid and sodium hydroxide. Surfactant of sodium lauryl sulfate (0.1 g/L) was added to prevent pinholes on the film surface. The total volume of the electro-plating solution was about 1 L, and plating occurred at 60 °C with 5 A/dm^2 current density.

The magnetoelectric measurement system is described in detail elsewhere [38]. The ME voltage coefficient was calculated based on $\alpha_E = \delta V/(t_{PZT} \cdot \delta H)$, where δH is the amplitude of the sinusoidal magnetic field generated by Helmholtz coils. For the plate sample, the polarization direction is along the PZT thickness (transverse direction), denoted as P in Fig. 1(a). We can obtain ME voltage coefficients effect of α_E^{T-L} and α_E^{T-T} when the magnetic fields are applied in the longitudinal and transverse directions, respectively. Magnetoelectric voltage coefficient α_E^{T-L} direction notation used in this paper is the following: the first superscript T denotes the transverse PZT polarization direction and L denotes the longitudinal magnetic applied direction. Similarly, α_E^{T-T} assumes that the PZT thickness is taken along the transverse plate direction, and the magnetic field is applied in the same plate transverse direction.

For these cylindrical layered samples, two ME voltage coefficients α_E^{R-A} and α_E^{R-V} were obtained corresponding to two conditions where H_{DC} and δH were applied along the cylinder axis, or in the vertical direction along its diameter, respectively. For α_E^{R-A}

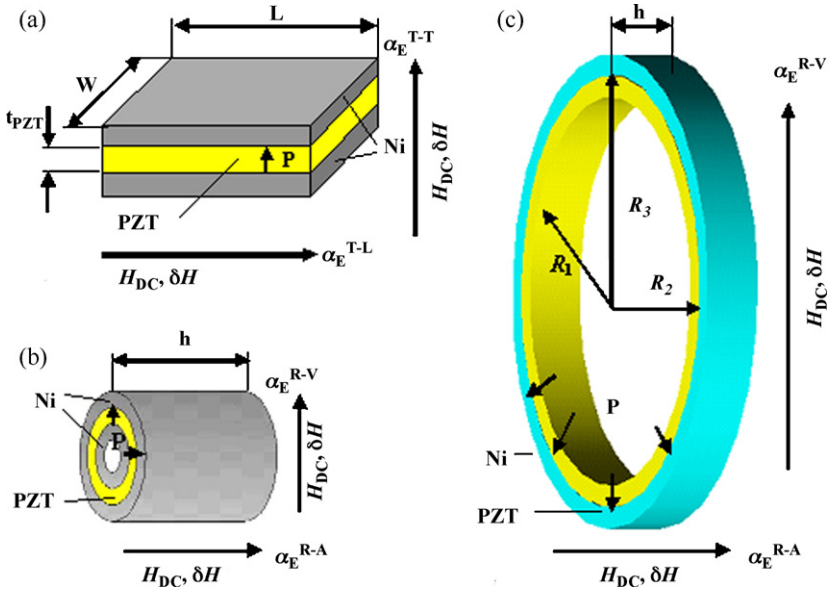

Fig. 1. Schematic of (a) planar trilayered Ni/PZT/Ni and (b) cylindrical trilayered Ni/PZT/Ni and (c) cylindrical bilayered Ni/PZT ME composite. Vector P shows PZT polarization direction. Other vectors identify the direction of applied magnetic field, and corresponding ME voltage coefficients.

Table 1
The main performance parameters of PZT-5H.

d_{33} ($\times 10^{-12}$ C/N)	d_{31} ($\times 10^{-12}$ C/N)	α ($\times 10^{-6}$ °C^{-1})	T_C (°C)	ε	K	tgδ	ρ (kg/m^3)	Q_m
500	−175	10	300	1750	0.65	0.02	7.5×10^3	50

and α_E^{R-V}, R denotes radial polarization direction, while A and V denote axial and vertical axis along which direction the magnetic field is applied.

3. Results and discussion

3.1. ME effect in the plate layered composites

Three plate structures with varying Ni layer thickness, shown schematically in Fig. 1(a), were tested in both longitudinal and transverse modes as a function of applied magnetic field amplitude and frequency. At 1 kHz magnetic field frequency it was found that the transverse ME voltage coefficient reaches a sharp peak at 4.5 kOe, while in the transverse mode the maximum was reached at 0.16 kOe [39].

Fig. 2 shows the magnetoelectric voltage coefficients of the 10 mm × 20 mm × 0.65 mm Ni/PZT/Ni composite structure shown schematically in Fig. 1(a) as a function of the applied magnetic field, H_{DC} in transverse (α_E^{T-T}) and longitudinal (α_E^{T-L}) directions. The total thickness of top and bottom Ni layers is 0.4 mm, and the data was obtained at 1 kHz magnetic field oscillation frequency. With the magnetic filed amplitude increase, the longitudinal α_E^{T-L} shows a sharp peak, reaching a maximum of 0.5 V/(cm Oe) at H_m = 0.16 kOe, then decreases rapidly to zero at 3 kOe. In contrast, the transverse α_E^{T-T} has two peaks, one at low H_{DC}, and a second maximum of 0.13 V/(cm Oe) at H_m = 4.5 kOe.

Fig. 3 compares the ME voltage coefficients frequency dependence of the trilayered Ni/PZT/Ni composite structure in longitudinal, α_E^{T-L} and transverse, α_E^{T-T}, directions obtained at corresponding optimized magnetic fields of 0.16 kOe and 4.5 kOe, respectively. The longitudinal α_E^{T-L} is much larger than the transverse α_E^{T-T}, although both peaks occur at the same resonant frequency. This means that regardless of the magnetic field application direction, the sandwich structure vibrates at its natural electromechanical resonance (EMR) frequency of 90 kHz. ME voltage coefficient magnitude and the field dependence are related to a variation of the demagnetization effect [40]. The magnetostrictive layer plate geometry dictates that the longitudinal line magnetostriction will be much higher than the transverse one, so the maximum of α_E is larger and the corresponding DC magnetic field

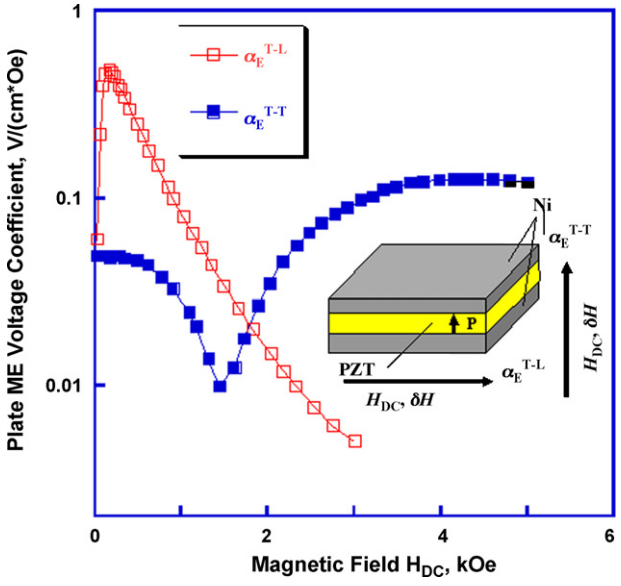

Fig. 2. Magnetoelectric voltage coefficient in transverse α_E^{T-T} and longitudinal α_E^{L-T} directions at room temperature for Ni–PZT–Ni trilayered composites with Ni layers thickness of 0.4 mm.

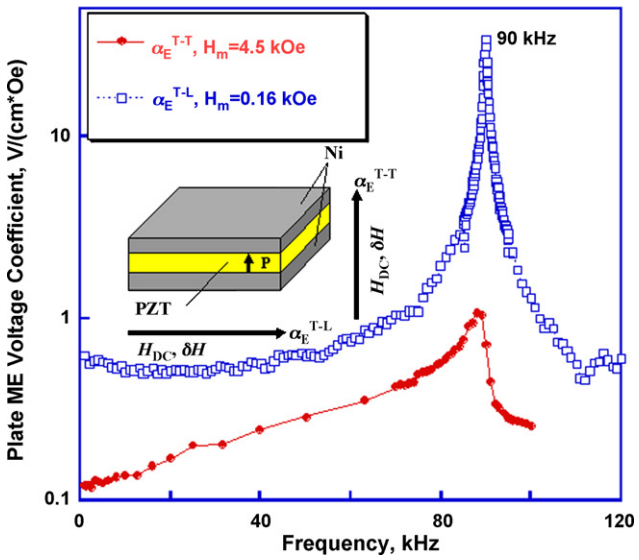

Fig. 3. Frequency dependence of the longitudinal and the transverse ME voltage coefficients for the Ni–PZT–Ni trilayered composite with 0.2 mm Ni layer thickness at H_m corresponding to the maximum ME coupling [39].

is lower. Srinivasan et al. also obtained a similar result [40]. PZT is not constrained in the transverse direction due to the layered plate structure geometry, thus it is under plane stress conditions.

We also measured the dielectric constant and the dielectric loss of the laminated Ni–PZT–Ni composite as a function of frequency, and found that the dielectric constant discontinuity happens at the resonance frequency of 90 kHz [39,41]. Fig. 4 shows the longitudinal ME coefficient, α_E^{T-L}, as a function of frequency for three samples with different Ni layer thicknesses, t_{Ni}. The EMR frequency shifts towards higher values with increasing Ni thickness due to the fact that thicker Ni is more efficient in straining PZT and the structure becomes stiffer [30]. According to Bichurin's theoretical model of the magnetoelectric resonance effect, the ME coefficient peak value is determined by the effective piezomagnetic and piezoelectric coefficients, compliance and permittivity [42]. H_{DC} curves of a plate layered ME composite shown in Fig. 2 indicate that the main difference between α_E^{T-T} and α_E^{T-L} is that while there is a sharp peak at low magnetic field for α_E^{T-L}, there is a broader peak at high

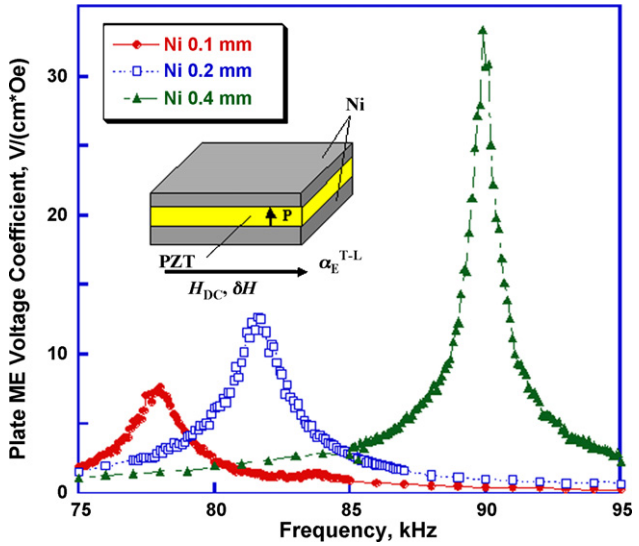

Fig. 4. Ni layer thickness effect on the ME voltage coefficient of the plate structure in the longitudinal mode [39].

field only for α_E^{T-T}. Dong et al. also obtained similar results for a plate structure [43]. As H_{DC} and δH are applied along the longitudinal direction, a sharp peak of α_E always appears at the low field. However, as H_{DC} and δH are applied along the transverse direction, a flat peak of α_E appears at the high field.

For the trilayered plate α_E^{T-L} measurement, the magnetic field direction is applied along the composite plate length (in-plane direction), but it is along the PZT thickness direction (out of plane) for α_E^{T-T}, which is aligned with the PZT polarization direction. Ni shrinks in the direction of the applied magnetic field. Absolute dimension change (shrinkage) due to the magnetostrictive effect is larger in the plane of the plate composite structure (when the magnetic filed is applied in the longitudinal direction) than in the transverse out-of-plane direction, since the in-plane dimension is larger in this case. That is why there is a sharp peak at H_{DC} applied in PZT polarization direction, while there is a broad peak in the direction perpendicular to the PZT polarization for the plate structure.

For the magnetoelectric layered structure, the interfacial bonding between magnetostrictive and piezoelectric layers is important to their ME performance. Liu et al. theoretically predicted the influence of interfacial bonding layer thickness and its shear modulus on the magnetoelectric effect [44]. With the interfacial binding layer thickness increase and its shear modulus decrease, the ME response will rapidly decrease. It is worth to note that the magnetostriction of Ni is two orders of magnitude smaller than that of the Terfenol–D, but the ME voltage coefficient of the laminated Ni–PZT–Ni composite synthesized by electrodeposition is comparable with that of the Terfenol–D/PVDF/PZT bulk samples because the adhesive Polyvinylidene Fluoride (PVDF) interfacial layer in the Terfenol–D/PVDF/PZT system is eliminated in the electrodeposited Ni–PZT–Ni system [29,45]. The shear modulus of metal is much higher than that of PVDF, and the metal layer bonds directly with PZT, without the need for adhesive PVDF bonding. Hence, better interfacial coupling between PZT and Ni layers offsets Ni's smaller magnetostriction compared with Terfenol-D. It is possible to enhance the ME coefficient further by polarizing PZT in the longitudinal direction and electrodepositing thicker metals with higher magnetostriction coefficient. We showed that thicker Ni layers results in higher ME voltage coefficient. The possible reason is that Ni has lower demagnetization factor than the Terfenol-D [46].

3.2. ME effect in cylindrical layered composites

Fig. 5 compares the ME voltage coefficients for trilayered and bilayered cylindrical composites obtained at 1 kHz applied magnetic field frequency. For the Ni/PZT/Ni cylindrical trilayered composite the PZT dimension are Ø 18 mm × Ø 20 mm × 8 mm. The trilayered cylinder axial H_{DC} curve is similar to that of a plate layered ME composites when the magnetic fields are applied in the longitudinal direction. There is a sharp peak at low field (below 0.5 kOe) in both axial and vertical modes observed in Fig. 5 for the trilayered cylinder. With the increased bias magnetic field the ME voltage coefficient decreases in the vertical mode, but there is a second wide maximum peak at 4.1 kOe [47].

Similar to the trilayered plate structure in the vertical direction, there are two peaks observed for the trilayered cylinder, one at low, and one at higher magnetic fields. The cylindrical ME composite can be divided into a series of infinitely small vertical units. In the axial mode, the fields are applied along the axis of each infinitesimal cylindrical unit, so a sharp α_E^{R-A} peak appears at low magnetic field, similar to the plate longitudinal mode. When the magnetic fields are applied perpendicular to the cylinder axis (vertical mode), the situation is more complex. In this condition, each infinitesimal unit slopes with the fields, and can be treated as a combination of two plate units, one parallel and another one normal to the fields. As a result, a sharp peak of α_E^{R-V} appears at a low applied magnetic field and a flat peak appears at a high field, similar to the sloping or the parallel combination of two plate structures.

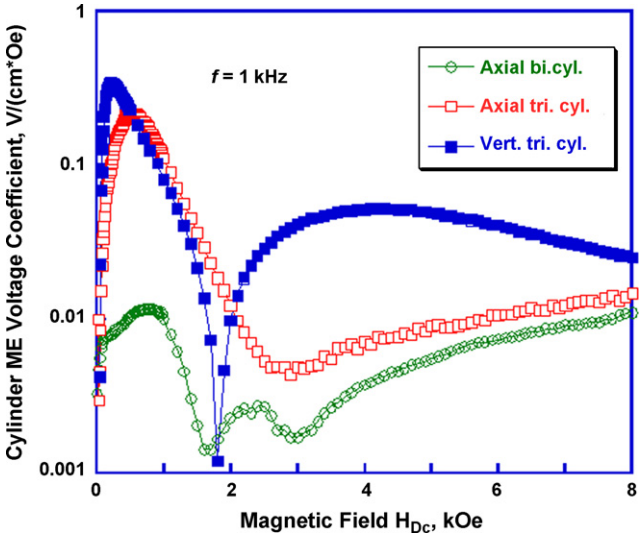

Fig. 5. Dependence of vertical trilayered cylinder, axial trilayered and bilayered cylinder ME voltage coefficients on the bias magnetic field H_{DC} at f = 1 kHz of AC field δH for the Ni-PZT cylindrical layered composites [37,39,41].

Fig. 6 shows cylindrical trilayered structure's α_E^{R-A} and α_E^{R-V} as functions of frequency measured at fixed bias fields. A sharp resonance peak at $f \approx 63.8$ kHz was detected for both directions, where the large ME coefficient is associated with the EMR [43]. A similar resonance was already analyzed in the plate trilayered composites. For the cylindrical ME composite with the thickness ratio of $t_{Ni}/(t_{Ni} + t_{PZT}) = 1/2$, the maximum ME voltage coefficient is $\alpha_E^{R-V} = 35\,V/(cm\,Oe)$ at 0.16 kOe, which is about two times larger than that of a plate trilayered composite with the same magnetostrictive-piezoelectric phase ratio, $\alpha_E^{T-L} = 16\,V/(cm\,Oe)$.

The ME effect for the cylindrical composites at low magnetic fields (<0.16 kOe) in the vertical mode is similar to that of the plate composites in the longitudinal mode, but it is similar to that of the transverse mode in high magnetic fields (>4.1 kOe). For a

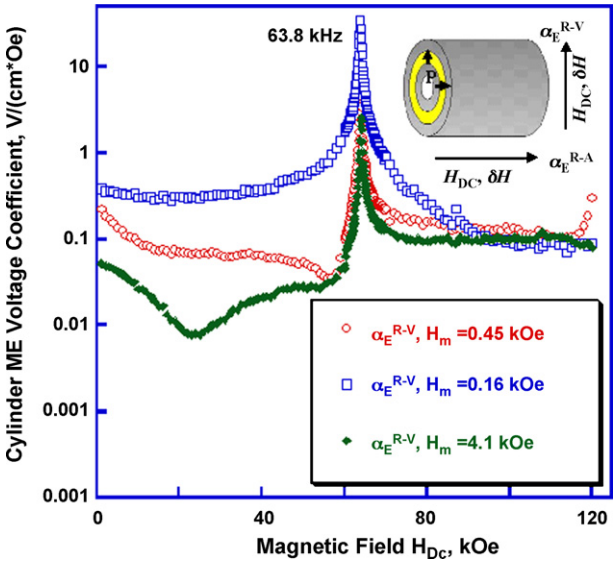

Fig. 6. Frequency dependence of the ME voltage coefficient for Ni–PZT–Ni cylindrical trilayered composite measured at different applied magnetic fields in axial and vertical directions [41].

plate composite, the longitudinal ME voltage coefficient is an order of magnitude larger than the transverse one [36]. The same reason is for the cylindrical structure vertical ME voltage coefficient at H_{DC} = 0.16 kOe being an order of magnitude lager than that at H_{DC} = 4.1 kOe in the vertical mode. However, for the axial, α_E^{R-A}, and the vertical, α_E^{R-V}, modes the different ME effects originate from the shape demagnetization influence on the magnetostrictive layers [40].

In our previous study, the cylinder can be simplified as an infinitesimally plate layered structure, the boundary conditions of the cylinder are not the same as those of the plate layered structure [48]. Both outer Ni layers of the plate structure are under plane stress conditions and are not constrained in the vertical direction (the free vertical state), while the cylinder outer and inner faces are constrained in the axial, radial and circumferential directions (the self-bound state). When the Ni ring shrinks (or expands) in the magnetic fields, not only does its circumference decrease (or increase) but also its diameter and height decrease (or increase) at the same time due to the self-bound effect. Then each PZT infinitesimal unit will suffer radial and tangential forces simultaneously due to the change in the shape of the NI layers. Two PZT modes of d_{33} and d_{31} contribute to the ME coefficient at the same time. Hence, the cylindrical layered ME composite can be simplified as a plate trilayered ME composite in the self-bound state [49].

The self-bound state can promote the ME effect in layered composites, which strongly depends on the mechanical coupling between the layers. Guo et al. reported that the clamped ME composites had a larger ME voltage coefficient than those in the free state [49]. The cylindrical shape forces its infinitesimal elements in the self-bound state naturally, therefore, we predicted that the cylinder would have a much larger ME voltage coefficient than the plate. The maximum of α_E^{T-L} was about 16 V/(cm Oe) for the plate sample, while the maximum of α_E^{R-V} is about 35 V/(cm Oe) for the cylindrical sample with the same magnetostrictive–piezoelectric phases thickness ratio [39,47]. Our experimental results are in good agreement with the theoretical predictions.

The dependence of α_E^{R-A} on bias magnetic field H_{DC} at f = 1 kHz for δH of a Ni/PZT cylindrical bilayered ME composite presented schematically in Fig. 1(c) with the dimension of Ø 18 mm × Ø 20 mm × 3 mm is shown in Fig. 5. It can be seen that α_E^{R-A} at 1 kHz has a maximum value at H_m = 0.6 kOe, and then continues to increase with increasing H_{DC} > 3 kOe.

The bilayered cylinder ME composite frequency dependence of α_E^{R-A} was measured at the bias field of H_{DC} = 0.6 kOe and H_{DC} = 6 kOe, respectively, shown in Fig. 7. For both H_{DC} = 0.6 kOe and H_{DC} = 6 kOe, there are sharp peaks at 60 kHz. The electromechanical resonance peak under high field of H_{DC} = 6 kOe is $\alpha_E^{R-A} = 21$ V/(cm Oe) and is much larger than that under low field of H_m = 0.6 kOe.

A linear relationship between the ME voltage coefficient and the magnitude of applied magnetic field at resonance frequency was observed [37]. Fig. 8 shows the bias field dependence of α_E^{R-A} at resonance frequency of 60 kHz for the bilayered cylindrical ME composite. It can be seen that the α_E^{R-A} increases linearly with increasing bias field above 1 kOe. This result was unexpected because the H_{DC} curve linearity does not exist in conventional (plate) layered composites whose ME voltage coefficient approaches zero at high bias magnetic fields. Therefore, we could not use the traditional theory to explain this phenomenon.

For ferromagnetic materials, like Ni, line magnetostriction $\lambda = \Delta l/l$ increases with increasing bias magnetic field, H_{DC}, then it reaches a saturation value λ_s at H_s. The volume magnetostriction changed with H_{DC}, when $H_{DC} > H_s$, the volume magnetostriction increased with increasing field H_{DC} when $H_{DC} < H_s$, the volume change $\omega = \Delta V/V$ is too small to be measured [50]. Under low magnetic field, i.e. $H_{DC} < H_s$, the field dependence of the ME voltage

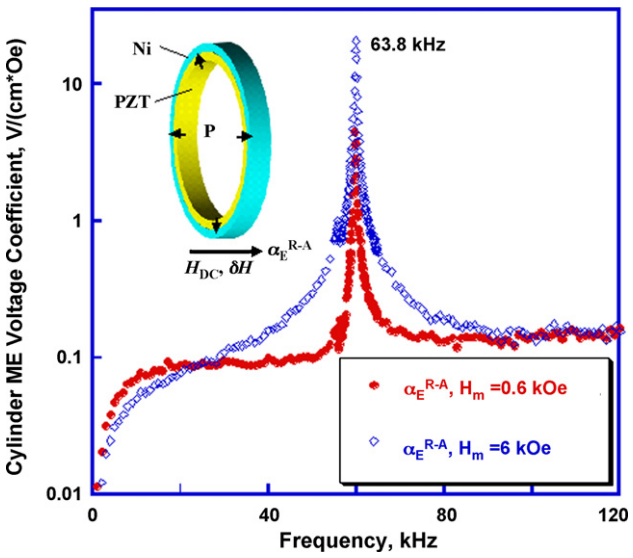

Fig. 7. Frequency dependence of the axial ME voltage coefficient, α_E^{R-A}, at 0.6 kOe and 6 kOe for Ni-PZT cylindrical bilayered composite.

coefficient is determined by the variation of the piezomagnetic coupling q with the field H_{DC}, and α_E is proportional to q, i.e. to $\delta\lambda/\delta H$, where $\delta\lambda$ is the differential magnetostriction. When $H_{DC} = H_s$, $\lambda = \lambda_s$ and then $\delta\lambda/\delta H = 0$, therefore, the $\alpha_{E(\omega)}$ caused by the line magnetostriction is equal to zero under high bias field. The volume magnetostriction of ferromagnetic Ni phase under high bias field of $H_{DC} > H_s$ can also generate strain in the PZT, resulting in increasing the voltage of δV across the PZT. Thus, $\alpha_{E(\omega)}$ induced by the volume magnetostriction appears under high bias field, which increases with bias magnetic field. The total ME effect is the sum of $\alpha_{E(\lambda)}$ caused by line magnetostriction under low fields and $\alpha_{E(\omega)}$ induced by volume magnetostriction under high fields, i.e. $\alpha_E = \alpha_{E(\lambda)} + \alpha_{E(\omega)}$. For a plate or disc trilayered composites, there is no constraint on the boundary of the ferromagnetic phase, and then no $\alpha_{E(\omega)}$ appears under high field, i.e. $\alpha_E = \alpha_{E(\lambda)}$. For the ring bilayered composite illustrated in Fig. 1(c), $\alpha_E = \alpha_E = \alpha_{E(\lambda)} + \alpha_{E(\omega)}$ and $\alpha_{E(\lambda)}$ plays the main

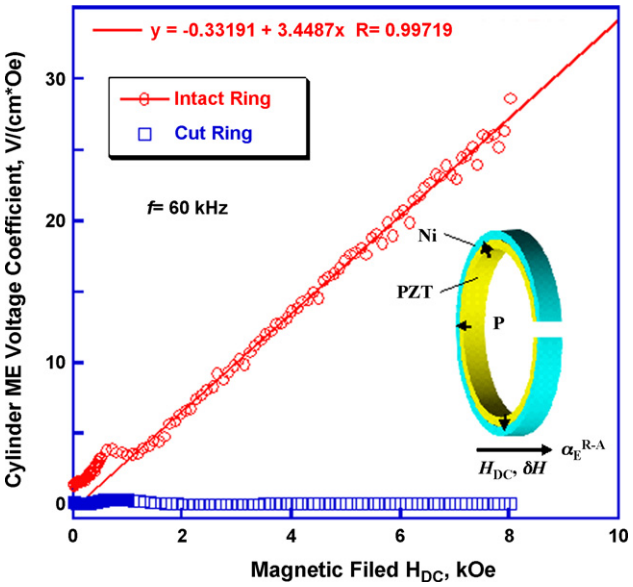

Fig. 8. Bias field H_{DC} dependence of the axial ME voltage coefficient, α_E^{R-A}, at 60 kHz resonance frequency for the intact and cut Ni-PZT cylindrical bilayered composite [37].

role under low bias fields, while $\alpha_{E(\omega)}$ plays the main role under high fields.

As shown in Fig. 8, the linearity of α_E and the bias magnetic field is 0.997 in the 2–8 kOe range. This result is unique because in previous reports the α_E decreased significantly when the external magnetic field was larger than 1 kOe for most conventional high-field magnetic sensors [51]. Based on these results, we can predict that the range of high linearity of the α_E and bias magnetic field in cylindrical composite should be wider, so the cylindrical composite will achieve a potential application in new generation of high-field magnetic sensors. As an additional proof that the cylinder bilayered structure exhibits giant ME effect due to its geometry, we cut the cylinder along its axial direction, which significantly reduced the circumferential and radial stresses in the structure. While the 60 kHz resonance frequency remained in the cut cylinder, the cut added other resonance frequencies of 60.5 kHz and 63.9 kHz, which correspond to other vibration modes. At the similar resonance magnetic field frequency of 60 kHz the ME voltage coefficient decreased orders of magnitude in high magnetic field, as seen in Fig. 8.

4. Conclusions

The method of electrodeposition was used to make layered magnetoelectric composites of varying geometry. The disadvantages of using an intermediate binder layer (nonrigid contact, fatigue and aging) were eliminated, which enhanced the magnetoelectric effect. Electrodeposited plate Ni/PZT/Ni layered composites have ME properties comparable with bounded Terfenol-D/PZT structures. Electrodeposition provides means for synthesizing various ME composites with complex geometries, so that better ME properties can be obtained though structural design.

Cylindrical layered composites have larger ME voltage coefficient compared to the plate layered composites due to their complex geometry. The longitudinal model of the plate structure is similar to the axial mode of the cylindrical composite. The linear relationship between α_E^{R-A} and H_{DC} after 1 kOe in cylindrical bilayered ME composite can be utilized in high magnetic field sensor applications. The improvement of preparation method may promote the development of ME composite towards practical applications.

Acknowledgments

This work was supported by the Major Program of the National Natural Science Foundation of China (Grant No. 50572006, 50802008 and 50874010), and by the Natural Science Foundation of Beijing, China (Grant No. 2073026), and by the Program for New Century Excellent Talents in University (Grant No. 20060420152), and by Scholars and Innovative Research Team in University (Grant No. 0509). Alex A. Volinsky would like to acknowledge support from NSF (Grant No. CMMI-0600266).

References

[1] N. Cai, J.Y. Zhai, Z. Shi, Y.H. Lin, C.W. Nan, Chin. Phys. 13 (2004) 1348.
[2] J. Zhai, S. Dong, Z. Xing, J. Li, D. Vieland, Appl. Phys. Lett. 91 (2007) 123513.
[3] G. Srinvasan, A.S. Tatarenko, M.I. Bichurin, Electron. Lett. 41 (2005) 10.
[4] C. Pettiford, S. Dasgupta, J. Lou, S.D. Yoon, N.X. Sun, IEEE Trans. Magn. 43 (2007) 3343.
[5] J.P. Zhou, Z. Shi, G. Liu, H.C. He, C.W. Nan, Acta Phys. Sin. 55 (2006) 3771.
[6] Y.K. Fetisov, G. Srinivasan, Appl. Phys. Lett. 88 (2006) 143503.
[7] N. Hur, S. Park, P.A. Sharma, S. Guha, S.W. Cheong, Phys. Rev. Lett. 93 (2004) 107207.
[8] R.C. Rai, J. Cao, J.L. Musfeldt, S.B. Kim, S.W. Chenong, X. Wei, Phys. Rev. B 75 (2007) 184414.
[9] V.J. Folen, G.T. Rado, E.W. Stalder, Phys. Rev. Lett. 6 (1961) 607.
[10] G.T. Rado, V.J. Folen, Phys. Rev. Lett. 7 (1961) 310.
[11] J. Wang, J.B. Neaton, H. Zheng, V. Nagarajan, S.B. Ogale, B. Liu, D. Viehland, V. Vaithyanathan, D.G. Schlom, U.V. Waghmare, N.A. Spaldin, K.M. Rabe, M. Wuttig, R. Ramesh, Science 299 (2003) 1719.
[12] J.F. Scott, Phys. Rev. B 16 (1977) 2329.
[13] H. Schmid, Bull. Mater. Sci. 17 (1994) 1411.
[14] C.W. Nan, Phys. Rev. B 50 (1994) 6082.
[15] J. Van Suchtelen, Philips Res. Rep. 27 (1972) 28.
[16] V.D. Boomgaard, R.A.G. Born, J. Mater. Sci. 13 (1978) 1538.
[17] R.S. Devan, B.K. Chougule, J. Appl. Phys. 101 (2007) 014109.
[18] C.W. Nan, M. Li, X.Q. Feng, S.W. Yu, Appl. Phys. Lett. 78 (2001) 2527.
[19] C.W. Nan, L. Liu, N. Cai, J. Zhai, Y. Ye, Y.H. Lin, L.J. Dong, C.X. Xiong, Appl. Phys. Lett. 81 (2002) 3831.
[20] C.W. Nan, N. Cai, L. Liu, J. Zhai, Y. Ye, Y. Lin, J. Appl. Phys. 94 (2003) 5930.
[21] J. Ma, Z. Shi, C.W. Nan, Adv. Mater. 19 (2007) 2571.
[22] G. Srinivasan, E.T. Rasmussen, J. Gallegos, R. Srinivasan, Y.I. Bokhan, V.M. Laletin, Phys. Rev. B 64 (2001) 214408.
[23] L. Li, Y.Q. Lin, X.M. Chen, J. Appl. Phys. 102 (2007) 064103.
[24] S.X. Dong, J.F. Li, D. Viehland, J. Appl. Phys. 95 (2004) 2625.
[25] C.W. Nan, G. Liu, Y.H. Lin, Appl. Phys. Lett. 83 (2003) 4366.
[26] N. Cai, C.W. Nan, J.Y. Zhai, Y.H. Lin, Appl. Phys. Lett. 84 (2004) 3516.
[27] J.G. Wan, J.M. Liu, H.L.W. Chand, C.L. Choy, G.H. Wang, C.W. Nan, J. Appl. Phys. 93 (2003) 9916.
[28] S.X. Dong, J.F. Li, D. Viehland, Appl. Phys. Lett. 85 (2004) 5305.
[29] Z. Shi, C.W. Nan, J. Zhang, N. Cai, J.F. Li, Appl. Phys. Lett. 87 (2005) 012503.
[30] J.G. Wan, Z.Y. Li, M. Zeng, H.H. Wang, J.M. Liu, Appl. Phys. Lett. 86 (2005) 202504.
[31] S.X. Dong, J.F. Li, D. Viehland, Appl. Phys. Lett. 84 (2004) 4188.
[32] S.X. Dong, J.F. Li, D. Viehland, Appl. Phys. Lett. 85 (2004) 2307.
[33] V.M. Laletin, N. Paddubnaya, G. Srinivasan, C.P. De Vreugd, M.I. Bichurin, V.M. Petrov, D.A. Filippov, Appl. Phys. Lett. 87 (2005) 222507.
[34] M. Bedenbecker, H.H. Gatzen, J. Appl. Phys. 99 (2006) 08M308.
[35] F.E. Rasmussen, J.T. Ravnkilde, P.T. Tang, O. Hansen, S. Bouwstra, Sens. Actuators A: Phys. 92 (2001) 242.
[36] A. Bai, C.C. Hu, Electrochem. Acta 50 (2005) 1335.
[37] D.A. Pan, Y. Bai, A.A. Volinsky, W.Y. Chu, L.J. Qiao, Appl. Phys. Lett. 92 (2008) 052904.
[38] J. Lu, D.A. Pan, Y. Bai, L.J. Qiao, Meas. Sci. Technol. 19 (2008) 045702.
[39] D.A. Pan, Y. Bai, W.Y. Chu, L.J. Qiao, J. Phys: Cond. Mat. 20 (2008) 025203.
[40] G. Srinivasan, C.P. De Vreugd, V.M. Laletin, N. Paddubnaya, M.I. Bichurin, V.M. Petrov, D.A. Filippov, Phys. Rev. B 71 (2005) 184423.
[41] D.A. Pan, Y. Bai, W.Y. Chu, L.J. Qiao, Smart Mater. Struct. 16 (2007) 2501.
[42] M.I. Bichurin, D.A. Filippov, V.M. Petrov, V.M. Laletsin, N. Paddubnaya, G. Srinivasan, Phys. Rev. B 68 (2003) 132408.
[43] S.X. Dong, J.Y. Zhai, F.M. Bai, J.F. Li, D. Viehland, J. Appl. Phys. 97 (2005) 103902.
[44] G. Liu, C.W. Nan, N. Cai, Y.H. Lin, J. Appl. Phys. 95 (2004) 2660.
[45] H. Yu, M. Zeng, Y. Wang, J.G. Wan, J.M. Liu, Appl. Phys. Lett. 86 (2005) 032508.
[46] S.Q. Ren, M. Wuttig, Appl. Phys. Lett. 92 (2008) 083502.
[47] D.A. Pan, Y. Bai, W.Y. Chu, L.J. Qiao, J. Phys. D: Appl. Phys. 41 (2008) 022002.
[48] D.A. Pan, S.G. Zhang, A.A. Volinsky, L.J. Qiao, J. Phys. D: Appl. Phys. 41 (2008) 205008.
[49] S.S. Guo, S.G. Lu, Z. Xu, X.Z. Zhao, S.W. Or, Appl. Phys. Lett. 88 (2006) 182906.
[50] C.W. Chen, Magnetism and metallurgy of soft magnetic materials, North-Holland publishing company, Amsterdam, New York, Oxford, 1977, pp. 75–78.
[51] J.E. Lenz, Proc. IEEE 78 (1990) 973.